Linköping Studies in Science and Technology
Licentiate Thesis No. 1292

Alumina Thin Film Growth: Experiments and Modeling

Erik Wallin

Linköping University
INSTITUTE OF TECHNOLOGY

LiU-TEK-LIC-2007:1
Plasma & Coatings Physics Division
Department of Physics, Chemistry and Biology
Linköping University, SE-581 83 Linköping, Sweden

ISBN: 978-91-85715-98-5
ISSN: 0280-7971

Printed by LiU-Tryck, Linköping, Sweden, 2007

ABSTRACT

The work presented in this thesis deals with experimental and theoretical studies related to the growth of crystalline alumina thin films. Alumina, Al_2O_3, is a polymorphic material utilized in a variety of applications, e.g., in the form of thin films. Many of the possibilities of alumina, and the problems associated with thin film synthesis of the material, are due to the existence of a range of different crystalline phases. Controlling the formation of the desired phase and the transformations between the polymorphs is often difficult.

In the experimental part of this work, it was shown that the thermodynamically stable α phase, which normally is synthesized at substrate temperatures of around 1000 °C, can be grown using reactive sputtering at a substrate temperature of 500 °C by controlling the nucleation surface. This was done by predepositing a Cr_2O_3 nucleation layer. Moreover, it was found that an additional requirement for the formation of the α phase is that the depositions are carried out at low enough total pressure and high enough oxygen partial pressure. Based on these observations, it was concluded that energetic bombardment, plausibly originating from energetic oxygen, is necessary for the formation of α alumina (in addition to the effect of the chromia nucleation layer). Further, the effects of impurities, especially residual water, on the growth of crystalline films were investigated by varying the partial pressure of water in the ultra high vacuum (UHV) chamber. Films deposited onto chromia nucleation layers exhibited a columnar structure and consisted of crystalline α-alumina if deposited under UHV conditions. However, as water to a partial pressure of 1×10^{-5} Torr was introduced, the columnar growth was interrupted. Instead, a microstructure consisting of small, equiaxed grains was formed, and the γ-alumina content was found to increase with increasing film thickness. When γ-alumina was formed under UHV conditions, no effects of residual water on the phase formation was observed. Moreover, the H content was found to be low (< 1 at. %) in all films. Consequently, this shows that effects of residual gases during sputter deposition of oxides can be considerable, also in cases where the impurity incorporation in the films is found to be low.

In the modeling part of the thesis, density functional theory based computational studies of adsorption of Al, O, AlO, and O_2 on different α-alumina (0001) surfaces have been performed. The results give possible reasons for the difficulties in growing the α phase at low temperatures through the identification of several metastable adsorption sites, and also provide insights related to the effects of hydrogen on alumina growth.

PREFACE

The work presented in this licentiate thesis constitutes the first part of my PhD studies in the Plasma & Coatings Physics group at Linköping University. The goal of my doctorate project, which is financially supported by the Swedish Research Council (VR), is to gain an increased understanding of alumina thin film growth. The results are presented in three appended papers, which are preceded by an introduction giving an overview of the research field and describing the methods used in the research.

Papers included in the thesis:

I. **"Phase control of Al_2O_3 thin films grown at low temperatures"**
J.M. Andersson, E. Wallin, U. Helmersson, U. Kreissig, and E.P. Münger
Thin Solid Films 513, 57 (2006).

II. **"*Ab initio* studies of Al, O, and O_2 adsorption on α-Al_2O_3 (0001) surfaces"**
E. Wallin, J.M. Andersson, E.P. Münger, V. Chirita, and U. Helmersson
Phys. Rev. B 74, 125409 (2006).

III. **"Influence of residual water on magnetron sputter deposited crystalline Al_2O_3 thin films"**
E. Wallin, J.M. Andersson, M. Lattemann, and U. Helmersson
Manuscript in final preparation.

Other papers, not included in this thesis:

"Effects of additives in α- and θ-alumina: an *ab initio* study"
E. Wallin, J.M. Andersson, V. Chirita, and U. Helmersson
J. Phys.: Condens. Matter 16, 8971 (2004).

"*Ab initio* calculations on the effects of additives on alumina phase stability"
J.M. Andersson, E. Wallin, V. Chirita, E.P. Münger, and U. Helmersson
Phys. Rev. B 71, 014101 (2005).

"Molecular content of the deposition flux during reactive Ar/O_2 magnetron sputtering of Al"
J.M. Andersson, E. Wallin, E.P. Münger, and U. Helmersson
Appl. Phys. Lett. 88, 054101 (2006).

"Energy distributions of positive and negative ions during magnetron sputtering of an Al target in Ar/O_2 mixtures"
J.M. Andersson, E. Wallin, E.P. Münger, and U. Helmersson
J. Appl. Phys. 100, 033305 (2006).

"Phase tailoring of Ta thin films by highly ionized pulsed magnetron sputtering"
J. Alami, P. Eklund, J.M. Andersson, M. Lattemann, E. Wallin, J. Bohlmark, P. Persson, and U. Helmersson
Thin Solid Films, *in press*.

ACKNOWLEDGEMENTS

Many people have supported me and contributed to this work in different ways. I would especially like to thank…

…my principal supervisor **Ulf Helmersson** for giving me the opportunity to perform this work and for his guidance, support, and encouragement during the last years.

…my co-supervisors **Valeriu Chirita** and **Peter Münger** for all their help with the theoretical part of this work and for always being open for discussions.

…**Jon Andersson** for introducing me to the alumina world, sharing his knowledge in the field, and for being a good friend.

…**Martina Lattemann** for invaluable help with TEM and for proof-reading this thesis.

…**Kalle Brolin, Thomas Lingefelt,** and **Inger Eriksson** for their technical and administrative skills.

…**the members of the Thin Film Physics and Plasma & Coatings Physics divisions** (past and present), as well as people from other groups at IFM, for experimental assistance, work and non-work related discussions at the coffee table, dinners, enjoyable traveling together, after-work beers, poker evenings...

…my **friends outside IFM** for always being there and for keeping my mind focused on something else every once in a while.

…my **parents**, last but definitely not least, for always supporting me and believing in me.

CONTENTS

1 INTRODUCTION

Aluminum oxide, or alumina for short, has the chemical formula Al_2O_3 and has been known and explored as a bulk material since antiquity, e.g., in the form of the gemstones sapphire and ruby [1]. (Sapphire and ruby are alumina doped with trace amounts of impurities giving rise to their characteristic colors.) Moreover, a stable, thin aluminum oxide scale forms naturally on metallic aluminum in air, protecting the aluminum from further oxidation and, consequently, being the reason for the good corrosion resistance of aluminum [2]. The development of aluminum oxide coatings has been pushed forward by, e.g., applications as protective coating in the cutting tool industry [3,4], as an insulating layer in semiconductor devices [5,6], and as tunnel barrier in special thin film structures [7,8]. As inferred from the above examples, alumina is a very well-researched material, but concerning the control and understanding of crystalline alumina thin film formation and properties many questions still remain to be answered. This is mainly due to the complexities arising from the existence of a wide range of different crystalline phases [9].

Industrially, protective alumina coatings on cemented carbide cutting tools, deposited using chemical vapor deposition techniques, have been used for several decades [3] and are still commonly applied and developed, due to the beneficial mechanical, chemical, and thermal properties of alumina [4]. The desire of being able to coat a wider range of materials with alumina films, and the wish to improve the properties of alumina coatings in general, has made many researchers try to deposit crystalline alumina using physical vapor deposition techniques, with the goal to, e.g., deposit the thermodynamically stable α phase, which is desirable in many applications, on heat sensitive substrates [10,11]. Application-wise, this is also one of the motivations for the present work. Besides this, being able to control the low-temperature synthesis of alumina in a better way might be beneficial in other applications. Of course, the fundamental knowledge gained from alumina as model system for oxide thin film materials in general could also be useful in many other situations.

The results of the thesis are presented in three appended papers treating different fundamental aspects of alumina thin film growth. In Paper I, the effect of controlled nucleation during reactive sputter deposition of alumina is explored. Paper II is a theoretical study of thin film growth related adsorption behavior on α-Al_2O_3 (0001) surfaces, while Paper III deals with experimental investigations of the effects of impurities, especially residual water, on the growth of crystalline alumina thin films. The outline of the introductory chapters preceding the papers are as follows. First an overview of thin film growth in general, and sputtering in particular, is given. After this, the analysis techniques used and the theory behind the computational modeling tools applied are presented. This is followed by a chapter devoted to the material alumina and an overview of previously published results related to alumina thin films and surfaces. The thesis is concluded with a summary of the results and a short outlook, where some ongoing and planned research is presented.

2 THIN FILM DEPOSITION

Thin films are used in a wide range of applications, e.g., as optical, electrical, decorative, and thermally or mechanically protective coatings. In this chapter some common methods for depositing thin films will be described, focusing on sputtering, which is the method of choice in this work.

2.1 Chemical and Physical Vapor Deposition

Thin film deposition techniques can be divided into two main categories; *chemical vapor deposition (CVD)* and *physical vapor deposition (PVD)*. In CVD, volatile gases (precursors) are let into the deposition chamber and are allowed to react in order to form the desired coating material on a substrate. This is normally done at elevated temperatures, meaning that the process takes place at, or close to, thermal equilibrium. CVD processes are commonly used in industry, e.g., for depositing alumina as a protective coating on cutting tools [3,4]. Among the drawbacks with the technique are the high temperatures used. This prohibits the use of heat sensitive substrates and might lead to problems when cooling down the substrates, due to, e.g., different thermal expansion coefficients of film and substrate. CVD techniques exist where one has tried to solve this problem, e.g., by using a plasma (instead of temperature) to activate the process (so called plasma assisted CVD).

In PVD techniques, material is instead vaporized (in vacuum) from a solid source and transported to the substrate, where it condenses to form a thin film. Hence, PVD processes can be used at significantly lower substrate temperatures compared to CVD, making it possible to perform depositions on heat sensitive substrates. It also means that the process can operate far from thermal equilibrium, allowing for, e.g., the formation of metastable phases. A range of different types of PVD methods exist. The most straight-forward ones rely on evaporation (or sublimation) of the source material. In this case, the material to be deposited is simply supplied with enough thermal energy in order to form a vapor, which then condenses on the substrates. However, with increasing demands on the quality of the coatings,

and with the desire to be able to deposit a wider range of materials, more flexible and efficient plasma-based PVD methods have been developed. Among these, arc evaporation and sputtering are the most common ones. In arc evaporation, a *high-current*, *low-voltage* discharge in the form of an arc spot is formed on the source. This causes local melting and evaporation of the material, as well as ejection of solid particles, which might lead to undesired incorporation of so called macroparticles in the coatings. However, the deposition rate is usually high and the technique is commonly used to deposit thicker coatings in industrial applications. Sputter deposition, on the other hand, relies on the ejection of the source material through ion bombardment, utilizing a *high-voltage*, *low-current* plasma discharge as described further below.

2.2 Sputtering

2.2.1 Basic Principles

The basic principle in sputtering relies on ejection (sputtering) of atoms from a source (usually called target) by bombardment of gaseous ions from a plasma (sometimes referred to as a glow discharge). The ejected atoms are then transported to the substrate, where they condense to form a film. The plasma is created by letting in a sputtering gas (usually a noble gas such as argon) in an evacuated vacuum chamber and applying a voltage between the target (cathode) and the chamber walls (anode). A schematic drawing of a typical sputter deposition system is shown in Figure 1. The applied voltage causes an avalanche effect in the gas, where the few electrons initially present in the gas are accelerated away from the cathode, eventually hitting gas atoms, ionizing them if the energy is high enough, and thereby creating more and more ions and electrons. If the conditions are suitable, a steady state will be reached where a partially ionized gas, a plasma, is sustained in the chamber.

2.2.2 The Sputtering Plasma

A plasma can be defined as a collection of free charged particles moving in random directions that is, on the average, electrically neutral [12]. Sputtering plasmas are usually weakly ionized, meaning that the ratio of charged particles to neutral particles in the quasi-neutral gas is small. Moreover, the low-pressure plasma discharges used in sputtering are electrically driven, and the much more mobile electrons are preferentially heated compared to the heavier neutrals and ions. Consequently, the average energy of the electrons, usually of the order of a few eV, is much larger than the average energy of the ions and neutrals, which is of the order

of a few tenths of meV. Hence, the discharge operates at a steady state far from thermal equilibrium.

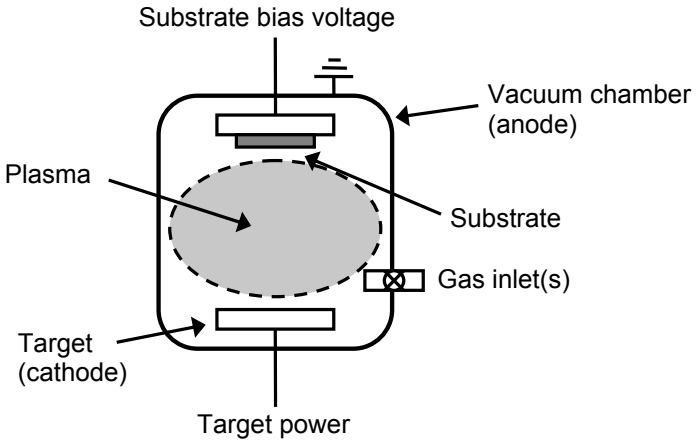

Figure 1. Schematic drawing of a simple sputter deposition system [13].

The plasma is at a constant potential, known as the *plasma potential*, V_p, which usually is the most positive potential in the system. This is due to the much higher mobility of the electrons compared to the ions, which causes an initial charge buildup on the anode and a corresponding electric field between the anode and the plasma as equilibrium is reached. The region between the chamber walls (or the surface of any other object immersed in the plasma) and the plasma is called the *plasma sheath*. This is where the potential drop occurs and, consequently, where the electric field is. Moreover, the high mobility of the electrons will cause any object immersed in the plasma which is electrically floating (such as, e.g., a substrate) to obtain a potential which usually is negative compared to both the plasma and anode potentials. This potential is known as the *floating potential*, V_f. Hence, ions leaving the plasma to an electrically floating substrate will be accelerated over a voltage, $V_p - V_f$, causing energetic bombardment of the growing film. The energy of this bombardment is often controlled by applying a *bias voltage* to the substrate, instead of having it electrically floating.

2.2.3 Processes at the Target

The positive ions in the plasma are attracted to the negatively biased cathode, sputtering away target atoms if the energy of the impacting ions is high enough. The efficiency of the process, i.e., the deposition rate, strongly depends on the *sputtering yield* of the target material. This

quantity is defined as the number of target atoms ejected per incident gas ion. The sputtering yield depends on a number of factors, such as the kinetic energy of the incoming atoms, the binding energy of the target atoms, the angle of incidence, and the efficiency of momentum transfer between the sputtering gas ions and the target atoms [14]. Besides ejection of target atoms, a number of other processes might occur as the energetic ions hit the target, as depicted in Figure 2. For example, crucial for maintaining a direct current plasma is the emission of secondary electrons from the cathode, which compensates for the electrons continuously lost to the chamber walls. The number of electrons emitted per incident sputter gas ion, known as the *secondary electron emission coefficient*, also proves to be important for the deposition rate. If the secondary electron emission coefficient is large, the current in the discharge will increase. At constant applied power (or when keeping the current constant), this means that the target voltage will decrease, causing a corresponding reduction in sputtering yield and deposition rate. How this influences the reactive sputtering process of alumina is further discussed in section 2.2.6.

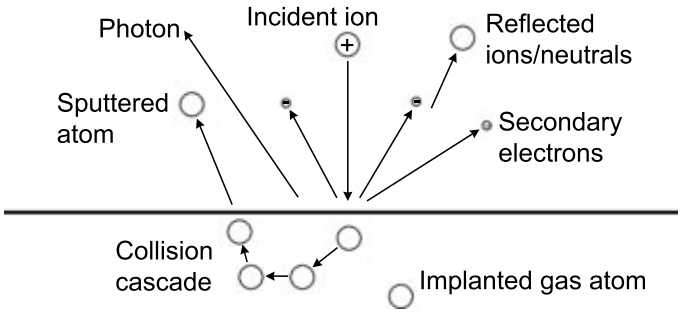

Figure 2. Different possible processes occurring at the target surface.

2.2.4 Magnetron Sputtering

To be able to achieve more efficient sputtering conditions, most modern sputter deposition systems utilize *magnetrons* [15]. In a magnetron, magnets are placed directly behind the target as shown in Figure 3. The electrons will then be acted on by the Lorentz force, given by

$$\mathbf{F} = q(\mathbf{E} + \mathbf{v} \times \mathbf{B}), \tag{2.1}$$

where q is the charge, $\mathbf{v}$ is the velocity of the particle, and $\mathbf{E}$ and $\mathbf{B}$ are the electric and magnetic fields, respectively. Hence, the magnetic field will cause the electrons to move in spiral shaped orbits around the magnetic field lines (if ejected non-parallel to the field). This

leads to a better confinement of the ionizing electrons close to the target in the region where the magnetic field lines are parallel to the target surface. The higher ionization probability in this region will lead to more efficient sputtering and a higher sputtering rate, resulting in the formation of an erosion track on the target surface (see Figure 3). Magnetrons make it possible to, e.g., run the process at a lower sputtering gas pressures, thereby enhancing the film properties. Of course, also the ions will be affected by magnetic forces, but due to the much larger mass of the ions compared to the electrons, this effect is usually negligible.

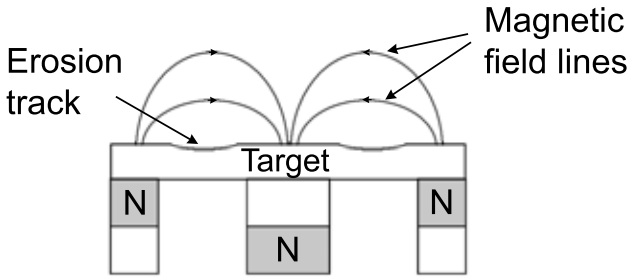

Figure 3. Schematic drawing of a magnetron.

2.2.5 DC and RF Sputtering

The most straightforward way to do sputter deposition is to apply a constant voltage between the target (cathode) and the chamber walls (anode). This is known as direct current (DC) sputtering. However, in some cases it is beneficial to instead use a time-varying voltage. For example, when reactively depositing an insulating material using a reactive gas and a metallic target, parts of the target surface might become covered with an insulating film (see section 2.2.6). This results in that a positive charge develops on the target surface, eventually causing the sputtering process to cease, or a dielectric breakdown (an arc) to occur on the surface. To prevent this, pulsed DC power can be applied [16]. In this technique, an asymmetric pulse is used, which discharges the surface during the positive cycle (usually 10-20 % of the total voltage cycle time). Typical frequencies are in the order of a few tenths or hundreds of kHz. Other applications of pulsed power include the recently developed high power impulse magnetron sputtering (HIPIMS) technique [17]. Here, very high power pulses with a low duty factor are used to produce a high density plasma, while still keeping the average power, and thereby the target heating, at a reasonable level. The high plasma density results in that a much higher fraction of the target material becomes ionized compared to conventional sputtering. This is beneficial in many applications.

When the target material one wishes to use is electrically insulating, a current can no longer be drawn through it and ordinary DC sputtering is impossible. However, one can still transfer energy to the plasma through capacitive coupling if high enough frequencies are used. The technique of applying sinusoidal radio frequency (RF) signals to the target is known as RF sputtering. At radio frequencies, the fields change quickly enough so that the heavier ions no longer can follow the fields, but slow enough so that the electrons can.* In this frequency regime, the electrons will oscillate with the applied field and transfer energy to the plasma through collisions, causing, e.g., ionization and excitation processes. The reason that sputtering actually takes place at the target is that a negative DC *self-biasing* will occur at the cathode relative to the anode. This is due to the higher mobility of the electrons compared to the ions, which will result in that an electron current is initially drawn to the electrodes as the time varying signal first is applied, causing a charge buildup on the surfaces as described in section 2.2.2. Since the electrodes are capacitively coupled to the plasma, and capacitance is directly proportional to electrode area, the voltage drop will be significantly larger at the target (cathode) compared to the chamber walls (anode). Hence, the resulting sputtering situation will be similar to that obtained with DC power. One of the drawbacks with RF sputtering in industrial applications is the more complicated and expensive equipment needed, e.g., in order to avoid reflections of power due to mismatching impedances, which might occur due to the high frequencies. In this work, RF power has been used both for reactive sputtering of an Al target in Ar/O_2 gas mixtures (Paper I) and for depositions from a ceramic Al_2O_3 target (Paper III).

2.2.6 Reactive Sputtering

When sputter depositing a compound, such as a nitride or oxide, two distinctly different methods exist. Either a compound target is used directly, or a metallic target together with a reactive gas such as oxygen or nitrogen is used. The latter method is known as reactive sputtering and is the preferable technique in many applications, since it allows for the use of DC, or pulsed DC, power instead of RF sputtering, and most often results in higher deposition rates. Usually, a mixture of an ordinary inert sputtering gas, such as argon, and the reactive gas is used. The lower deposition rates obtained with compound targets are, e.g., in the case of alumina, due to both the higher surface binding energies of the target atoms, and the higher secondary electron emission coefficient of alumina, causing a lower target voltage at constant current or power.

* The frequency 13.56 MHz is reserved for these purposes and is therefore most often used.

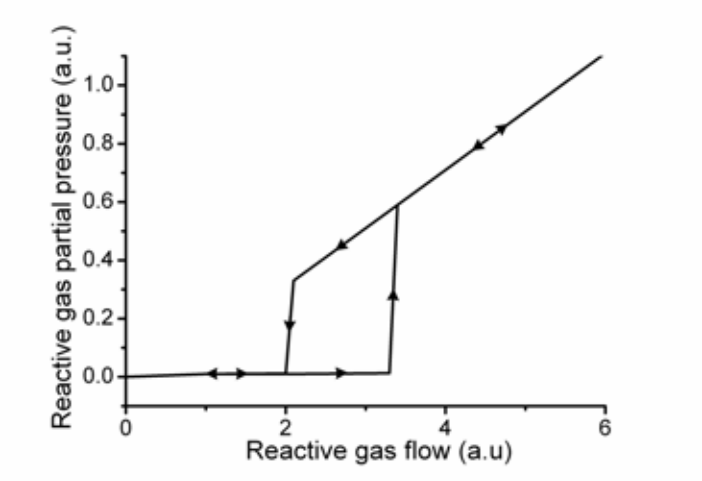

Figure 4. Typical hysteresis behavior of the reactive gas partial pressure as the reactive gas flow is varied.

Due to reactions occurring between the reactive gas and the continuously deposited chamber walls and substrate, the reactive sputtering process becomes rather complicated and much effort has been put into finding ways of effectively controlling the process [18]. The reactive sputtering process has also been successfully modeled by Berg *et al.* [19]. The complexity of the process is caused by the apparently conflicting demands of depositing stoichiometric films, while still avoiding the formation of a compound phase on the target (so called *target poisoning*). Hence, a too low reactive gas flow will lead to the formation of understoichiometric films, whereas a too high gas flow will result in the formation of a compound also on the target surface, causing arcing on the target surface or a reduction in deposition rate for the same reasons as when depositing from a compound target directly. Figure 4 shows a typical reactive gas partial pressure versus reactive gas flow graph. The increase in reactive gas partial pressure is negligible as the reactive gas is first introduced, due to gas consumption caused by compound formation between the sputtered metal and the reactive gas at chamber walls and the substrate. However, as a certain threshold value is reached the chamber walls become saturated and the pressure rises quickly. Above this limit, the partial pressure will vary linearly with the reactive gas flow. If the pressure is decreased again, the drop to a lower partial pressure will often occur at a lower gas flow than the sudden increase did, forming a *hysteresis* curve. Recent additions to the Berg standard model have shown that the hysteresis effect can be reduced, and even completely eliminated, if a small enough target size (or, rather, target erosion zone), or a high enough pumping speed, is used

[20]. In this work, reactive sputtering was utilized in Paper I. Due to the high pumping speed and small target size of the laboratory scale deposition system used for these experiments, essentially no hysteresis effects were observed.

3 ANALYSIS TECHNIQUES

In order to study how different parameters affect the growth, it is, of course, necessary to be able to study the properties of the grown films, such as crystal structure and microstructure. Moreover, to understand the growth evolution, it is in many situations beneficial to be able to characterize the plasma and the deposition flux in various ways. In this chapter, the tools used for these kinds of analyses in the appended papers will be briefly described.

3.1 Plasma Analysis

Different properties of the plasma, such as the plasma and floating potentials, are conveniently measured using plasma probe techniques, which in principle rely on measuring voltage-current characteristics for differently designed conducting probes immersed in the plasma [21]. To be able to characterize the species in the deposition flux, however, more complicated measurement techniques are needed. In this work, the method known as mass spectrometry was applied.

3.1.1 Mass Spectrometry

Mass spectrometers are used in many applications within physics, chemistry, and biology, e.g., to find the composition of unknown samples. In this work, mass spectrometry was used in Paper III to measure the composition of the ion flux incident onto the substrate. The mass spectrometer used in this study, a Hiden PSM 003, is differentially pumped in order to allow for measurements at the higher chamber pressures typically used during sputter deposition and has a probe with a small orifice (0.3 mm in diameter) sticking into the plasma. The basic function of mass spectrometers is based on filtering ions with respect to their mass-to-charge ratio, using electric and magnetic fields. Since electric and magnetic field are used to guide the particles, they need to be charged. This means that if neutrals are to be studied, they need to be ionized first, while, e.g., the ion flux from a plasma can be measured directly. The mass spectrometer used in Paper III has an ionization stage, which can be activated when measur-

ing neutral species. The ionization stage consists of a filament ejecting electrons, which are accelerated to a certain energy and subsequently ionize the neutrals through impact ionization. The ionized species then pass through a few extraction electrodes, of which the voltages can be tuned to optimize detection for the conditions in a certain measurement situation. In some spectrometers, referred to as energy-resolved mass spectrometers, this stage is followed by a unit filtering ions with respect to their kinetic energy. This is the case for the spectrometer used in this work, and it utilizes a so called Bessel box for the energy filtering. The final stages are the ion mass-to-charge filtering and the detection, both of which can be done in numerous different ways. In the present case, the mass filtering was performed by a *quadrupole mass filter*, which consists of four electrodes to which radio frequency power with a superimposed direct current voltage is applied in a sophisticated way, resulting in that only ions with the desired mass-to-charge ratio will pass. Finally, the detection was done with a *secondary electron multiplier*. Mass spectrometry is a very powerful technique in many cases, but it should be emphasized that it is mainly a *qualitative technique*, and that quantitative evaluation of measurements is a very delicate matter.

3.2 Thin Film Characterization

There are many characterization methods available to study different properties of thin films. In this work, three main techniques have been used; x-ray diffraction to study the crystal structure of the films, transmission electron microscopy to investigate their microstructure and crystallinity, and elastic recoil detection analysis to study the composition of the deposited samples. These three methods are described in the following sections.

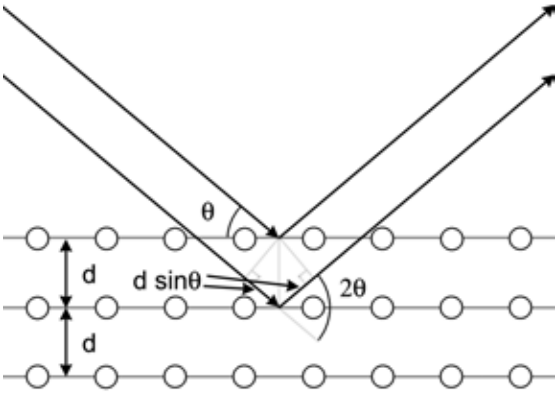

Figure 5. Schematic illustration of diffraction according to Bragg's law.

3.2.1 X-ray Diffraction

In x-ray diffraction (XRD), an x-ray beam is incident onto the sample and the *diffracted* beams coming out of it are detected. The intensity of the diffracted radiation is dependent on the interaction of the beam with the sample and, in particular, the orientations of, and distances between, different crystallographic planes. A schematic illustration of the principle of the technique is shown in Figure 5. By requiring that the difference in path length of beams diffracted from different atomic planes should equal an integer number of wavelengths, i.e., for constructive interference to occur, Bragg's law can be derived. Bragg's law gives a condition for intensity maxima of the diffracted radiation as a function of the angle θ, and is given by

$$2d \sin\theta = n\lambda, \tag{3.1}$$

where n is an integer, λ is the wavelength of the x-ray radiation, and d is the interplanar spacing of the diffracting atomic planes. Of course, the situation in a real sample is more complicated than in the schematic shown in Figure 5. Still, this model is applicable in most cases.

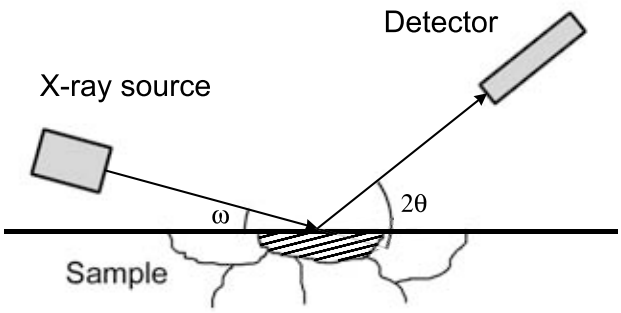

Figure 6. Schematic illustration of an x-ray diffraction setup.

A schematic illustration of a practical XRD setup is shown in Figure 6. Often, both the angle of the incident beam, $\omega(=\theta)$, and the diffraction angle, 2θ, are scanned simultaneously in a coupled manner forming a so called $\theta/2\theta$ scan. In this case, only planes parallel to the sample surface are probed. However, for the study of thin, polycrystalline films like in the present work, it might be beneficial to instead use grazing incidence XRD (GIXRD) [22]. In this method, the angle of the incident beam, ω, is kept at a small angle (usually a few

degrees) relative to the sample surface, and only the diffraction angle, 2θ, is varied. In this way, the penetration depth of the beam is reduced and data from a larger sample area is obtained, resulting in a relative increase in the diffracted intensity from the near-surface part of the sample. Note that for GIXRD, the orientation of the probed atomic planes relative to the sample surface is different throughout the scan.

XRD methods can be used to determine a number of thin film properties, such as crystal structure, grain size, stress, and preferred growth directions [23] and XRD is, consequently, a very powerful technique. The advantages of the method include the fact that it is a *non-destructive* method, and that it requires no, or very limited, sample preparation. Moreover, due to the relatively large area hit by the incident x-ray radiation, it is a *macroscopic* method, contrary to, e.g., transmission electron microscopy. In this work (Papers I and III), GIXRD was used to determine the phase composition of grown films by comparing diffractograms (detected intensity versus diffraction angle) with available published data for different alumina phases.

3.2.2 Transmission Electron Microscopy

In transmission electron microscopy (TEM) [24], electrons are used to produce images by letting an electron beam pass through a sample and detecting the transmitted electrons. Due to the wavelike properties of matter, electrons with the energies typically used in TEM can be associated with wavelengths in the order of 10^{-12} m. Hence, this enables imaging at resolutions far superior to other microscopy techniques, such as, e.g., ordinary optical microscopy. However, TEM is a complicated method, where high quality electromagnetic lenses have to be used to focus the electron beam, and where the studied specimen has to be thin enough so that electrons can pass through it. Consequently, TEM requires expensive equipment, a skilled operator, as well as extensive sample preparation.

There are several different ways of obtaining images in TEM. The most straightforward way is to detect the directly transmitted beam. This yields what is known as a *bright field image*. This was used in Paper III, e.g., for creating cross-sectional high resolution images of the Cr_2O_3/Al_2O_3 interface as exemplified in Figure 7. The incoming electron beam is also *diffracted* in a similar way as x-rays. These diffracted beams can be used to generate an electron diffraction pattern, containing information of, e.g., the crystal structure of the studied sample. Often, an aperture of a certain size is inserted so that diffraction information is obtained from a more limited region of the sample. This is known as *selected area electron diffraction* (SAED) and was used in Paper III to study the evolution of the crystal structure with film thickness. Furthermore, it is possible to generate images from one or more of the

diffracted beams, yielding *dark field images*. These can, e.g., be used to image grains with a certain crystallographic orientation. Such imaging was used to study the columnar grain structure of some of the films investigated in Paper III.

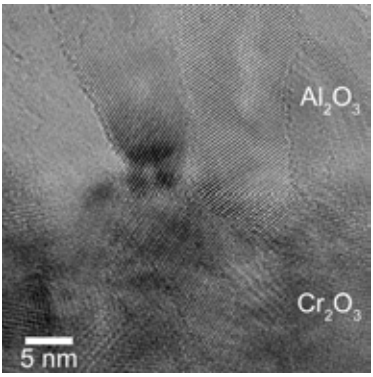

Figure 7. Cross-sectional high resolution transmission electron micrograph of a Cr_2O_3/α-Al_2O_3 interface. From Paper III.

Preparing TEM specimens is somewhat of an art, and there are many possible ways to do it. The cross-sectional specimens investigated in this work, such as the one shown in Figure 7, were prepared by first cutting the deposited sample into pieces approximately 1×2 mm, and placing two such pieces in a Ti grid with the film sides facing each other. The sample was then first mechanically thinned and polished, and thereafter ion milled to electron transparent thickness using a GATAN Precision Ion-Polishing System (PIPS). A final polishing step using low-energy ions was performed in order to remove the damaged surface layer caused by the preceding step.

3.2.3 Elastic Recoil Detection Analysis

Knowing the chemical composition is of crucial importance in order to understand the properties of thin films. However, quantifying the elemental composition of compounds is not straightforward, especially not for materials consisting of relatively light elements such as alumina. Consequently, many standard techniques are difficult to use in a quantitative way. Elastic recoil detection analysis (ERDA), however, allows for reliable quantification of aluminum and oxygen, as well as hydrogen, in thin film samples [25]. In ERDA, the studied sample is exposed to a beam of highly energetic ions (in the present work Cl^{7+} ions with an energy of 35 MeV was used) at an angle with respect to the surface. This results in that the lighter film atoms are forwardly scattered away from the surface (recoiled) through essentially

elastic collisions. By detecting the mass and energy of the recoiling species, a depth-resolved composition profile can be obtained. In Papers I and III, ERDA was used to study the aluminum, oxygen, and hydrogen content of the films. The recoiled aluminum and oxygen species were detected in a Bragg ionization chamber, whereas hydrogen was measured with a Si detector. In these measurements, the composition was found to be fairly constant throughout the film thickness. Therefore, only average values are presented in the appended papers.

4 THEORETICAL MODELING

Theoretical tools, in particular the ones relying on a quantum mechanical description of the systems under study, have had a tremendous impact on materials research during the past decade. In this chapter, the theory behind some of these computational tools will be outlined, focusing on methods based on the density functional theory.

4.1 Background

The motivation for using computer codes in materials science in the first place is, at least, two-fold. Firstly, calculating material properties with theoretical tools might give the researcher the possibility to understand the system on a much smaller geometrical scale, or much shorter time scale, than what is possible experimentally. Secondly, using computers can make it possible to simulate experiments, or series of experiments, which are too time consuming, too expensive, or too dangerous to perform in real life. Overall, the information gained from the calculations can be of great value when trying to explain or predict experimental results.

The modeling can be carried out using a number of methods of different sophistication, resulting in different accuracy and computer demands of the programs. The key issue in any atomistic computer simulation of a material is to find a good-enough description of the interaction between the atoms. Depending on how this interaction is calculated, the computational methods can be divided into two main categories; classical and quantum mechanical methods. In a classical description, forces between atoms are described by an interaction potential, represented by an analytical formula with parameters typically derived empirically from experimental results. Hence, this description might work reasonably well for situations closely resembling the conditions during the experiments on which the fit was based. However, one has to be careful when using the potential in other, untested situations. In quantum mechanical methods on the other hand, the forces and bonding between atoms are calculated from purely theoretical considerations of the electronic structure of the material

and the only information needed by the computer program is the atomic number of the species involved. Since no fitting to known material data is needed, the quantum mechanical methods are also referred to as *ab initio* (Latin meaning *"from the beginning"*) or *first principles* methods. The main disadvantage with quantum mechanical calculations is that they are very computationally demanding, consequently putting limitations on the system sizes and time scales which are possible to study.

When the forces acting on the atoms are known, the desired physical information can be obtained in different ways. One can, e.g., let the atoms relax according to the calculated forces to obtain an (0 K) equilibrium configuration corresponding to a local or global minimum in the potential energy of the system. In other methods, one studies the time evolution of the system at a certain temperature (as in molecular dynamics, MD, methods), or statistical averages of properties from an ensemble of systems (as in Monte Carlo, MC, simulations). In this work, the modeling has been carried out using density functional theory based quantum mechanical calculations of the total energy and electronic structure of equilibrium configurations. The rest of this chapter will therefore be devoted to this methodology and, in particular, density functional theory (DFT). (For a more thorough description, see, e.g., the textbook by Martin [26].) In Paper II, DFT was used to study the adsorption behavior of possible film forming species on different α-Al_2O_3 (0001) surfaces.

4.2 Density Functional Theory

4.2.1 The Hohenberg-Kohn Theorems

In general, solving a problem quantum mechanically means solving a Schrödinger equation with $3N$ degrees of freedom, where N is the number of particles. In materials research, N translates to the number of electrons in the system, which means that solving this equation turns into an extremely numerically demanding task even for small systems. The foundation for an alternative approach called density functional theory was laid in the 1960s through two theorems presented and proved by Hohenberg and Kohn [27]. The two theorems can be stated as follows:

1. For a system of interacting particles in an external potential, $V_{\text{ext}}(\mathbf{r})$, the external potential is uniquely determined (except for a constant) by the ground state particle density, $n(\mathbf{r})$.
2. The total energy of the system can be described by a functional of the particle density, $E[n(\mathbf{r})]$, with the ground state energy of the system being the minimum of this func-

tional. The particle density minimizing $E[n(\mathbf{r})]$ is the exact ground state particle density.

Of course, in most materials applications particles mean electrons. The first theorem tells us that the full Hamiltonian is known if $n(\mathbf{r})$ is known, since the external potential is fully determined by the ground state electron density. Consequently, all properties of the system are in principal determined by the ground state electron density. The second theorem tells us that $n(\mathbf{r})$ can be determined if $E[n(\mathbf{r})]$ is known for the system. However, formulating $E[n(\mathbf{r})]$ is generally not straightforward, and effective approximations are needed to make use of the theory in practice.

4.2.2 The Kohn-Sham Equations

The first step towards practical applications of DFT was taken by Kohn and Sham [28]. They based their approach on the assumption that the exact ground state electron density can be represented by the ground state density of another, auxiliary system of *non-interacting* electrons. The validity of this assumption has so far not been rigorously proven in the general case, but methods relying on it have been found to work very well. Using this approach, the Kohn-Sham energy functional can be written as

$$E_{\mathrm{KS}}[n(\mathbf{r})] = T_{\mathrm{s}}[n(\mathbf{r})] + \int V_{\mathrm{ext}}(\mathbf{r}) n(\mathbf{r}) d\mathbf{r} + E_{\mathrm{Hartree}}[n(\mathbf{r})] + E_{\mathrm{xc}}[n(\mathbf{r})], \tag{4.1}$$

where $T_{\mathrm{s}}[n(\mathbf{r})]$ is the kinetic energy of the system of non-interacting electrons, $V_{\mathrm{ext}}(\mathbf{r})$ is the external potential, and $E_{\mathrm{Hartree}}[n(\mathbf{r})]$ represents the Hartree energy, which is the classical approximation of the electron-electron interaction. The many-body effects known as exchange and correlation are grouped into the last term, $E_{\mathrm{xc}}[n(\mathbf{r})]$. This quantity cannot be calculated exactly in the general case, but different approximations can be applied in order to estimate it. A few of these approximations are discussed in section 4.2.3.

Knowing the explicit form of the energy functional, the total energy can be minimized in order to arrive at the ground state electron density and the ground state energy. This is often done with respect to the Kohn-Sham wave functions, $\psi_i(\mathbf{r})$, which are related to the electron density through

$$n(\mathbf{r}) = \sum_{i=1}^{N} |\psi_i(\mathbf{r})|^2 . \tag{4.2}$$

Minimizing the total energy using a variational approach leads to a set of Schrödinger-like equations known as the Kohn-Sham equations,

$$\left[-\frac{\hbar^2}{2m}\nabla^2 + V_{\text{eff}}(\mathbf{r})\right]\psi_i(\mathbf{r}) = E_i\psi_i(\mathbf{r}), \tag{4.3}$$

where $V_{\text{eff}}(\mathbf{r})$ is an effective potential including the external potential, as well as Hartree and exchange-correlation terms corresponding to equation (4.1). Hence, the original 3*N* dimensional problem has been formulated as a set of equations involving only three variables. For this achievement and the development of DFT in general, Walter Kohn was awarded the Nobel Prize in chemistry in 1998 [29]. The task of DFT computer codes is to solve this set of equations in order to yield the correct ground state electron density and total energy. Note that the equations have to be solved self-consistently, since $V_{\text{eff}}(\mathbf{r})$ depends on the electron density and, consequently, $\psi_i(\mathbf{r})$.

4.2.3 Approximations for the Exchange-Correlation Energy

The exchange-correlation energy, $E_{\text{xc}}[n(\mathbf{r})]$, can be approximated in a number of different ways. In the simplest approach, which was presented already in the seminal paper by Kohn and Sham [28], one simply replaces the exchange-correlation potential at a certain point in space with that of a homogenous electron gas having the same density. This approach is known as the *local density approximation* (LDA) and yields surprisingly good results in many situations.

The most straightforward extension to the LDA is to include a dependence of one more term in the Taylor series expansion of the electron density, i.e., a gradient term. This approach is known as the gradient expansion approximation (GEA) and was also suggested in the original paper of Kohn and Sham [28]. However, it most often leads to worse results than the LDA [30]. Therefore, approximations have been designed where the behavior of the gradient behavior is adjusted so that the exchange-correlation functional preserves certain desired properties. These are known as *generalized gradient approximations* (GGAs). There exist numerous different GGAs. Three commonly used forms are the ones by Becke (B88) [31], Perdew and Wang (PW91) [32], and Perdew, Burke, and Ernzerhof (PBE) [33]. In this work, the PW91 functional was applied.

4.2.4 Plane Waves and Pseudopotentials

In order to solve the Kohn-Sham equations numerically, the unknown wave functions are expanded in a basis of some known basis functions. When describing solids subject to periodic boundary conditions, a natural choice is to use a basis set consisting of plane waves. However, of course one cannot use an infinite number of plane waves, and the series expansion consequently has to be truncated at some point. The number of plane waves included in this expansion is one important parameter to consider when performing plane wave DFT calculations in practice.

One simplification commonly applied in order to keep the computational cost at a reasonable level is the so called *frozen-core approximation*. This approximation relies on the fact that the core states are not affected by chemical bonding to any great extent, while at the same time being costly to describe using plane waves. The frozen-core approximation solves this problem by only calculating the properties of the core electrons once, and keeping them fixed during the rest of the calculations. The core region is then commonly described using *pseudopotentials*. It is important that these pseudopotentials yield smooth wave functions for the valence electrons in the core region, so that the wave functions can be accurately described using a reasonable number of plane waves. A range of different approaches to this problem exists. Two commonly used methods are the ultrasoft pseudopotential (USPP) method [34] and the projector augmented-wave potential (PAW) method [35,36]. In Paper II, the PAW approach was used.

5 ALUMINA

In this chapter, selected alumina phases and their properties will be described. Also, a literature review of previous results concerning alumina thin film growth and alumina surfaces is presented.

5.1 Alumina Phases and their Properties

Besides the thermodynamically stable α phase, numerous metastable phases exist [9]. The different phases have differing properties, which is one of the reasons for the broad applicability of alumina. In the following sections, α-alumina and a few of the most relevant metastable phases are described.

Table 1. Selected properties of (bulk) α-alumina (at room temperature).

Property	Value	Reference(s)
Density (g/cm^3)	3.96-3.99	9, 40
Melting point (°C)	~2050	40
Bulk modulus (GPa)	239	37
Elastic modulus (GPa)	409-441	38, 40, 41
Hardness (GPa)	28	38
Thermal conductivity (W/(m·K))	46	41
Relative dielectric constant	10.5	41
Band gap (eV)	8.8	39

5.1.1 The α phase

The α phase of alumina, also known as *corundum*, is the only thermodynamically stable alumina phase. Some of its properties are summarized in Table 1. As can be seen, α-alumina is thermally stable and possesses very good mechanical properties. The appealing mechanical properties are preserved also at higher temperatures [40]. These properties combined with its chemical inertness have made it one of the technologically most important ceramic materials.

Moreover, it is an excellent electric insulator and optically transparent [41], making it useful for certain applications in electronics and optics. In its single crystal form, α-alumina is known as sapphire and is a commonly used substrate material, e.g., in optics and electronics.

The crystal structure of α-alumina can be described as an approximately hexagonal close packed (hcp) oxygen sublattice, with aluminum atoms filling two thirds of the octahedrally coordinated interstitial positions [42]. This structure, which is often referred to as the corundum structure, is shared with a number of other metal sesquioxides, such as Cr_2O_3, Fe_2O_3, and Ti_2O_3. The primitive unit cell is rhombohedral, and contains six oxygen atoms and four aluminum atoms. Often, however, the structure is more conveniently described by a hexagonal unit cell containing thirty atoms, due to the hcp arrangement of the oxygen anion sublattice, as shown in Figure 8. The [0001] direction of the hexagonal unit cell coincides with the [111] direction of the primitive rhombohedral cell. The lattice parameters are a = 5.128 Å and α = 55.3° in the rhombohedral representation, which transfers to a' = 4.76 Å and c = 13.0 Å for the hexagonal cell [42]. The bonding in α-alumina, and in alumina phases in general, is highly ionic with calculated effective ionic charges of close to +3 and -2 for aluminum and oxygen, respectively [43].

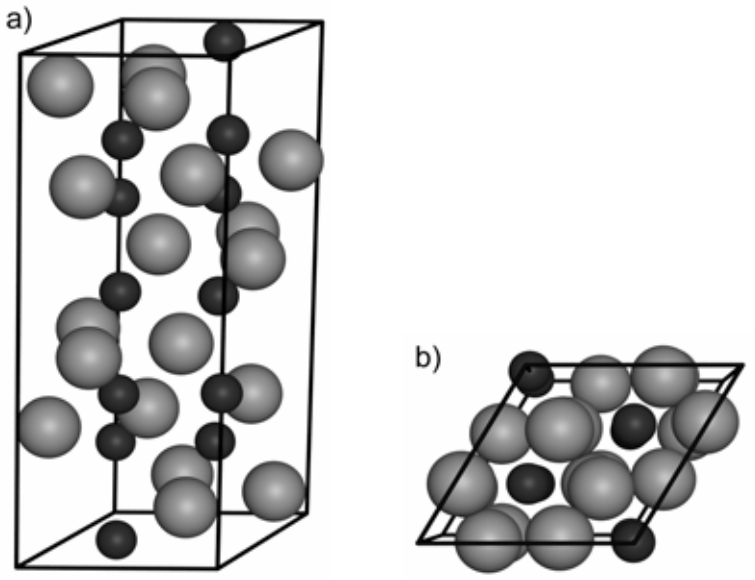

Figure 8. Side view (a) and top view (b) of the hexagonal unit cell of α-alumina. The smaller, darker spheres represent aluminum atoms and the larger, brighter ones oxygen atoms.

5.1.2 Metastable Phases

The number of reported metastable alumina phases, also known as *transition aluminas*, exceeds ten, although some of the phases reported in literature appear similar [9]. Among the metastable phases, subcategories can be defined based on the arrangement of the close-packed oxygen sublattice. For example, some phases have an approximately hcp arrangement of the oxygen anions (i.e., ···ABAB··· layer stacking), while others have a face centered cubic (fcc) arrangement (···ABC··· stacking). α-alumina belongs to the first category together with the χ phase, whereas, e.g., γ-, η-, δ-, and θ-alumina belong to the latter subcategory [9]. κ-alumina is often assigned to the first category, but the structure has more recently been determined to be orthorhombic with an approximate ···ABAC··· oxygen plane stacking [9,44] and should consequently more correctly be described as having a double hexagonal close packed (dhcp) oxygen structure. All metastable aluminas transform upon heating, with transformation sequences irreversibly ending in the thermodynamically stable α phase at elevated temperatures. The α-alumina transformation temperature is, however, relatively high, and it is possible to form many of the metastable phases at synthesis conditions between room temperature and about 1000 °C. This might pose a problem, e.g., when one wants to synthesize the α phase in a controlled way at low or intermediate temperatures, but it also opens the possibility to use the different transition aluminas in specific applications. The structures and transformation temperatures for some of the more commonly encountered metastable alumina phases are summarized in Table 2. It can be noted that the structures of many of the metastable phases commonly used in applications still are under debate. For example, it was not until recently that the κ phase structure was elucidated through a combination of experimental work and first principles calculations [44]. A similar approach has been used to yield a better description of the distribution of aluminum atoms in γ-alumina [45,46].

Table 2. Structure of, and transformations between, the bulk forms of some common metastable alumina polymorphs [9,41].

Phase	O sublattice	Transformation temperature (°C)	Transforms to
η	···ABC···	600-800	θ
γ	···ABC···	700-800	δ/θ
δ	···ABC···	900-1000	θ
θ	···ABC···	1000-1100	α
χ	···ABAB···	650-750	κ
κ	···ABAC···	900-1050	α
α	···ABAB···	2050	Liq.

The metastable phases find use in numerous applications. For example, chemically vapor deposited κ-alumina has, alongside α-alumina, been used extensively for wear-resistant coatings on cutting tools, since it forms easier than the α phase under certain CVD process conditions [47,48] (see section 5.2.1 for a more thorough discussion of CVD of alumina). The low surface energy and the consequent inherent high specific surface areas of the γ phase have made it useful in catalysis applications [9,49]. Here, the phase transformations occurring in high-temperature applications at 700-800 °C constitute a problem. Therefore, many attempts have been made to increase the thermal stability of this phase, e.g., by doping [9,50,51]. Furthermore, thin films consisting of (metastable) amorphous alumina has also proved to be useful, e.g., in optics and as a dielectric medium in electronics. In such applications, the alumina films are usually either deposited by sputtering [52] or by the CVD technique known as atomic layer deposition (ALD) [53].

5.2 Growth of Crystalline Alumina Thin Films

5.2.1 Chemical Vapor Deposition

Chemically vapor deposited α- and κ-alumina has been used for several decades as protective coatings on cemented carbide coating tools [3,4]. Most often, α-alumina is the preferred phase, mainly because of its thermal stability, but the κ phase is easily formed and has been used extensively [54]. Due to the good mechanical properties and relatively high transformation temperature, the κ phase performs as well as α-alumina in some applications [55]. However, as the cutting temperatures become high enough, the κ- to α-alumina transformation inevitably occurs. Due to the volume contraction accompanying the phase transformation, this results in severe cracking of the coating, causing an increase in wear rate [56,57]. One important factor influencing which phase that forms has been shown to be the nucleation surface on which the alumina coatings are deposited [58] and recent developments for CVD alumina has mainly been based on a better understanding of the effects of nucleation layers, not only for the phase formation, but also for the preferred orientation of the grown films [4]. It has been suggested that previous α phase CVD coatings in fact in many cases were coatings which had nucleated as κ-alumina, and subsequently transformed to α-alumina upon heating during, or after, the deposition [4]. Consequently, by more carefully controlling the nucleation stage of growth and promoting α phase nucleation, higher quality coatings have been obtained [4]. The cutting performance of the coatings has been shown to be further enhanced by promoting a certain texture by providing appropriate nucleation conditions [4]. Moreover, γ-alumina can be formed during CVD processes, even though it is seldom beneficial consider-

ing the applications in question. It has been shown that the formation of this phase is promoted by introducing H_2S as a catalyst and/or dopant during the depositions [59,60].

Although chemically vapor deposited alumina films dominate the market for alumina coated cemented carbide cutting tools, they still have drawbacks, mainly associated with the high deposition temperatures necessary (usually around 1000 °C). For example, the elevated temperatures might induce unwanted chemical effects due to reactions between substrate and film [61], and cracks might occur when the samples are cooled down after deposition, due to differences in the thermal expansion of the substrate and film materials [62]. Furthermore, the high deposition temperatures of course severely limit the choice of substrate materials to those withstanding high temperatures, such as, e.g., cemented carbides. To meet the need for lower deposition temperatures, alumina growth by plasma enhanced CVD (PECVD) has been studied by, e.g., Kyrylov *et al.* [63]. It was shown that by applying power densities of up to 6.6 W/cm^2 to the cathode (where the substrates were placed), α-alumina coatings could be deposited at substrate temperatures down to 580 °C. This was attributed to an increased adatom mobility caused by the energetic bombardment.

5.2.2 Arc Evaporation

Arc evaporation has an inherently high ionized fraction of the deposition flux and a high energy of the depositing species compared to, e.g., conventional sputtering [17]. Several authors have tried to utilize this, most often in conjunction with a fairly high substrate bias, in order to achieve and study low-temperature growth of crystalline alumina phases. For example, Brill *et al.* [64] deposited films containing α-alumina at substrate temperatures of 600-700 °C by applying a substrate RF bias voltage of -200 V. Films deposited with a substrate bias of less than -50 V only contained the α phase at temperatures above 800 °C and were found to be x-ray amorphous at temperatures below 400 °C. The coatings synthesized at intermediate temperatures contained a mixture of crystalline phases. Growth of crystalline alumina at comparable temperatures was reported by Yamada-Takamura *et al.* [65]. They performed TEM investigations of the α phase dominant films, revealing that the film growth started out as γ-alumina, with subsequent nucleation and growth of α-alumina on the γ phase at a film thickness of a few hundred nanometers. Rosén *et al.* [66] deposited alumina using a similar approach, but were not able to deposit phase pure α-alumina films with -100 V bias even at 800 °C. However, films dominated by the γ phase were synthesized at temperatures down to 200 °C. They attributed the apparent discrepancies compared to previous studies to differences in deposition conditions and possible influence of the choice of substrate on the phase formation.

5.2.3 Sputtering

Formation of crystalline phases utilizing conventional sputtering, without any special preparation of the nucleation surface, takes place at substrate temperatures above 400-500 °C [67,68,69], while alumina deposited at lower temperatures usually is x-ray amorphous. Most often, the crystalline phase formed is γ-alumina [67,70] and obtaining the α phase is not straightforward. However, the performance of sputter deposited γ-alumina coatings in, e.g., high speed metal cutting applications has been found to be surprisingly good [70].

In order to lower the formation temperature of crystalline phases in general, and α-alumina in particular, several authors have used different techniques to increase the ionized fraction of the material to be deposited (so called ionized PVD, IPVD). For example, Schneider *et al.* [71,72] used an RF coil to increase the ionization of the deposition flux and deposited films containing κ- and θ-alumina at temperatures down to 320 °C and 180 °C, respectively, by adjusting the ion flux to the substrate. More recently, Khanna and Bhat demonstrated growth of γ-alumina without intentional substrate heating utilizing hollow cathode magnetron sputtering [73]. Zywitzki *et al.* [10,74] deposited alumina with conventional pulsed DC sputtering and showed that practically phase pure α-alumina could be formed at 760 °C and the γ phase at temperatures down to 350 °C, if a suitable substrate bias and cathode power was applied. Using TEM, they showed that the α-alumina dominant films started growing as γ-alumina on the substrate, and that the α phase did not nucleate and start to grow until after a certain thickness [75]. Hence, these observations are very similar to those made for arc evaporated films by Yamada-Takamura *et al.* [65]. Li *et al.* [76] used an approach similar to that of Zywitzki *et al.*, but also employed a solenoid creating a magnetic field in the vicinity of the substrate, as well as higher substrate bias values (up to 400 V). They claimed to have synthesized (unidentified) crystalline alumina phases at temperatures down to 250 °C. However, some films went through partial amorphization within a couple of days after the depositions, plausibly due to the large compressive stresses present in the coatings.

The reasons for the difficulties in forming α-alumina during thin film growth at low or intermediate temperatures are not completely understood. However, the nucleation stage of growth has, similarly as in CVD, been shown to be important. For example, it was shown by Jin *et al.* [77] that by depositing a Cr_2O_3 (chromia) nucleation layer, α-alumina could be deposited by RF sputtering of a ceramic target at 400 °C. Cr_2O_3 has the same (corundum) structure as α-Al_2O_3 with a relatively small lattice mismatch, and is therefore expected to facilitate the nucleation of the α phase. The method was later shown to work for technological

substrates and the growth temperature was further lowered to 280 °C [78], indicating that the main obstacle for low-temperature α-alumina growth in fact is to nucleate the correct phase. Furthermore, it was suggested that surface energy stabilization of the γ phase could be the reason for the difficulties in initially nucleating α-alumina [78] (see section 5.3.2). Evidence for localized epitaxial growth of α-alumina onto the chromia grains was provided using TEM (see also Paper III) [78]. Kohara *et al.* [79] used a similar approach, but created the Cr_2O_3 nucleation layer by oxidizing a CrN layer predeposited onto the cemented carbide substrates. In Paper I, the conditions for deposition of α-alumina onto Cr_2O_3 nucleation layers by reactive sputtering of a metallic target were explored, and in Paper III, chromia layers were used in the study of effects from residual water on the growth of crystalline alumina phases.

5.3 Alumina Surfaces

5.3.1 Clean Surfaces and Surface Adsorption

Alumina surfaces in general, and α-alumina surfaces in particular, have been studied intensely in the past by both experimental and theoretical means. This has been motivated by the importance of alumina surfaces in applications, such as in catalysis and when used as substrate material. Moreover, the α-Al_2O_3 (0001) surface often serves as a prototype for oxide surfaces in general. In most reports, this surface is identified as the most stable α-alumina surface [80,81]. However, due to the ···O-Al-Al-O-Al-Al··· layer stacking sequence in the [0001] direction (cf. Figure 8), different terminations of this surface are possible, and the stable termination as well as the surface relaxations have been a matter of controversy in previous investigations [82,83,84]. Hydrogen on the surfaces has been found to be one important reason for the apparent discrepancies between different studies [85,86,87]. While the surface terminated by a single Al layer seems to be most stable under ultra high vacuum conditions, hydrogen on the surface might stabilize the O terminated surface and change the amount and direction of the surface relaxations [85,86,87]. More recently, γ-alumina surfaces have gained interest in theoretical studies, mainly due to an increased understanding of its structure, making, e.g., adsorption studies possible [51,88,89]. The γ phase has lower surface energy than the α phase, as shown both theoretically and experimentally [88,90]. This is the main reason for the inherent high specific surface areas and porous structures of γ-alumina, making it useful in catalysis applications (see also section 5.3.2).

Previous adsorption related studies have mainly been concerned with α-alumina surfaces and, in particular, the (0001) surface. For example, Lodziana and Norskov [91] studied the interaction of Cu and Pd with differently terminated (0001) surfaces and found that is was

weak and covalent-like for the Al-rich surface, whereas a stronger and ionic-like interaction was observed on the O terminated surface. Other authors have made studies of the interaction between other metal atoms, or metal surfaces, and α-Al_2O_3 surfaces and have found similar trends [92,93]. Rosén *et al.* [94] performed thin film growth related computational studies of adsorption of different Al and O ions on the O terminated surface. They found that the adsorption energies depended strongly on the adsorption site as well as on the charge state of the adsorbing ion.

5.3.2 Surfaces and Alumina Thin Film Growth

Surfaces are, of course, of crucial importance for thin film growth. For example, much of the structure of the resulting films is dependent on the mobility of adatoms on the growing surface. The mobility is affected by both the energy of the adatoms, which, e.g., can be supplied thermally or by energetic bombardment, and on the energy barriers for different surface diffusion processes. The only investigation related to surface self-diffusion on α-alumina surfaces known to the author is the theoretical study by Rosén *et al.* [95]. They used DFT calculations to estimate the diffusion barriers for Al^+ ions on the O terminated (0001) surface and found the activation energy for diffusion from a metastable site to the bulk Al position to be 1.6 eV. This was suggested as a possible explanation for the difficulties in growing the α phase at lower temperatures [95]. An increased adatom surface mobility is also often mentioned as a mechanism promoting α phase formation when depositing with assistance of energetic bombardment [63,66,76]. However, relatively high ion energies are in many cases required (often exceeding 100 eV [64,65,66,76]) and, consequently, additional mechanisms might very well be active. Moreover, it is not yet clear how a limited mobility can explain the apparent preference for γ-alumina formation as compared to the α phase.

A possible explanation for the preference for γ-alumina formation during physical vapor deposition of alumina has been elucidated recently. McHale *et al.* [90] measured the surface energies of γ- and α-alumina and found that for specific surface areas larger than 125 m^2/g, the γ phase is energetically favored compared to α-alumina, due to its significantly lower surface energy. Assuming spherical grains, 125 m^2/g corresponds to a grain size of ~13 nm in diameter. Hence, as also pointed out by Andersson *et al.* [78], the γ phase is in fact thermodynamically favored at small enough grain sizes, e.g., at the nucleation stage of thin film growth. This observation is further corroborated by TEM investigations of arc evaporated and sputter deposited α-alumina coatings, showing how γ-alumina nucleated on the substrate surface and how a gradual transition to α-alumina growth occurred [65,75].

6 SUMMARY OF RESULTS

In this chapter the main findings of the three appended papers are summarized and the motivation for the studies is outlined.

6.1 Paper I

As described in section 5.2.3, controlling the nucleation stage of growth has been shown to be crucial in order to form the α phase at lower temperatures during sputter deposition. Jin *et al.* [77] were first to demonstrate low temperature growth onto a Cr_2O_3 nucleation layer, and later the temperature was further lowered and the Cr_2O_3/Al_2O_3 interface closer investigated by Andersson *et al.* [78]. In both studies, RF sputtering of ceramic Al_2O_3 targets was applied. The purpose of Paper I was to investigate *reactive sputter deposition* of α-alumina onto chromia layers. Depositions were performed using RF sputtering of a metallic aluminum target at a substrate temperature of 500 °C, varying the total pressure as well as the oxygen partial pressure. It was found that the α phase could only be grown at a low enough total pressure and high enough oxygen partial pressure (i.e., in the poisoned mode), otherwise γ-alumina was formed. Based on these observations, it was concluded that energetic bombardment, plausibly originating from energetic oxygen, was necessary for the formation of α-alumina (in addition to the effect of the chromia nucleation layer). Later, energetic bombardment (i.e., a low enough total pressure) was shown to be a key issue also when depositing from a ceramic target (see Paper III). Energetic oxygen species with energies corresponding to acceleration over the target voltage (i.e., a few hundred eV) have previously been shown to be present during sputter deposition of oxides [96,97]. These form as negative oxygen ions at, or in the vicinity of, the target surface and are accelerated over the target sheath voltage. Some of them are neutralized on their way to the substrate [98]. That energetic oxygen indeed was the origin of the observed effects in this case was corroborated by energy-resolved mass spectrometry studies of the deposition flux performed parallel to the work presented in this thesis [99]. Some initial studies of the effects of residual water on the growth are also

presented in Paper I. The investigation of such effects is further extended and described in Paper III.

6.2 Paper II

Studies of alumina surfaces and surface processes on an atomic scale are an important step towards a better understanding of alumina thin film growth and phase formation. In Paper II, density functional theory based methods were used to study the adsorption of Al, O, AlO, and O_2 on differently terminated α-alumina (0001) surfaces. The three surface terminations obtainable by cleaving the bulk structure (AlO, AlAl, and O terminations), as well as a completely hydrogenated O terminated surface were considered. Al was found to adsorb strongly on the AlO and O terminated surfaces and showed a predominantly ionic-like interaction with the surfaces. The adsorption was stronger on the O terminated surface, where also several metastable sites were identified. On completely hydrogenated surfaces, Al adsorption in the bulk position was found to be unstable or very weak, depending on the configuration of the hydrogen surface atoms. O adsorption was unstable relative to molecular O_2 on the AlO terminated surface, whereas the interaction with the AlAl surface was shown to be considerably stronger. On this surface, dissociative adsorption of O_2 without any appreciable barrier was observed. On the O terminated surface, the creation of O vacancies was found to be plausible, corroborating earlier findings of a driving force towards O deficient configurations of this surface [85]. Concerning alumina thin film growth, the identification of several metastable adsorption sites on the O terminated surface provides a possible part of the explanation for the difficulties in growing crystalline alumina. Moreover, the results provide important insights into how hydrogen adsorption on growth surfaces might disturb the growth (see also Paper III).

6.3 Paper III

Previous studies of magnetron sputter deposited *amorphous* alumina thin films have demonstrated the importance of residual water for the resulting film properties. For example, a correlation between hydrogen incorporation and elastic modulus has been shown [100], and the mechanism of hydrogen incorporation has been investigated [101]. Furthermore, the role of the energetic bombardment in the α phase formation during PVD growth is not clear, and possible explanations include creation of lattice distortions (strains), facilitation of diffusion processes, and removal of impurities (e.g. hydrogen) on the growth surfaces. Hence, a study of how impurities, and in particular residual water, affect the growth of *crystalline* alumina

phases is highly motivated. In Paper III, growth of films under different vacuum conditions has been mimicked by varying the partial pressure of H_2O in the ultra high vacuum chamber. Films were deposited at a substrate temperature of 500 °C, both onto predeposited chromia nucleation layers, and directly onto silicon substrates. As expected, the films grown on chromia nucleation layers exhibited a columnar structure and consisted of crystalline α-alumina if deposited at a low enough total pressure under ultra high vacuum conditions. However, as water to a partial pressure of 1×10^{-5} Torr was introduced, the columnar growth was interrupted and a more porous microstructure consisting of small, equiaxed grains was formed. This microstructure change was accompanied by a change in the phase composition of the films, where the γ-alumina content was found to increase with increasing film thickness, as determined by XRD and SAED. Mass spectrometry of the ion flux to the substrate showed a significant increase of (energetic) negative ions (especially OH^-) as the water partial pressure was increased. Based on this, it was suggested that the change in film structure was due to one, or a combination, of at least two effects; (i) H adsorbing on growth surfaces, causing renucleation of grains with limited epitaxial relationship with the underlying grains (cf. Paper II), and (ii) renucleation due to an increased energetic bombardment caused by target surface reactions. Films deposited at higher total pressures, or without chromia nucleation layers, were found to consist of γ-alumina regardless of the water partial pressure. The fact that the γ phase formed as the total pressure was increased indicates that the energetic bombardment shown to be necessary during reactive sputter deposition of the α phase in Paper I, is also crucial when depositing from ceramic targets. ERDA showed that the H content was low (< 1 at. %) in all films, and that the H incorporation was varying only slightly with the water partial pressure. Consequently, this shows that effects of residual gases during sputter deposition of oxides can be considerable, also in cases where the impurity incorporation in the films is found to be low.

7 ONGOING AND FUTURE RESEARCH

Luckily, since the work presented in this thesis is planned to be the first part of a PhD thesis, some questions still remain to be answered and new ones have arisen. In this chapter, a few of the ongoing and planned projects are presented.

- As mentioned previously, computational studies of alumina surface processes on an atomic scale can provide a better understanding of alumina growth. The adsorption studies presented in Paper II is an important step towards this understanding. However, more valuable knowledge concerning thin film growth would be gained by studying barriers for kinetic processes, such as surface diffusion. Such studies are planned to be conducted using DFT in combination with the so called nudged elastic band method [102]. Some initial calculations of Al diffusion on different α-alumina (0001) surfaces have already been started. Moreover, it would of course be beneficial to carry out similar studies for other α-Al_2O_3 surfaces and for surfaces of other alumina phases.

- To allow for better comparisons between experiments and the calculations described in the preceding paragraph, it would be beneficial to study growth of more well-defined surfaces. A possible way to do this is to deposit alumina onto single crystal sapphire substrates, and study how different growth parameters affect the single crystal growth.

- The role and consequences of the bombardment found necessary for α-alumina formation in previous studies are not completely clear. For example, the use of ion energies of a few hundred eV is likely to influence the evolution of film stresses. Hence, studies of the correlation between film stresses, deposition parameters, and other film properties such as the phase composition, would be relevant. Moreover, the energetic oxygen found necessary for α-alumina formation in Paper I, has shown to cause compressive film stresses during growth of other oxides [103]. Preliminary results from *in situ* laser curva-

ture measurements indicate that the situation is similar for reactively sputter deposited alumina.

- In the past, some of the more successful attempts of low-temperature growth of alumina using sputtering have involved some form of additional ionization of the deposition flux. A very promising technique to achieve this, pioneered in the Plasma & Coatings Physics division at Linköping University, is high power impulse magnetron sputtering (HIPIMS) [17]. It would be very interesting to investigate if the use of this method is beneficial when synthesizing alumina thin films.

8 REFERENCES

[1] W.H. Gitzen, *Alumina as a ceramic material* (The American Ceramic Society, Westerville, 1970), p. 3.

[2] K.R. van Horn (Ed.), *Aluminum, Vol. 1: Properties, Physical Metallurgy and Phase Diagrams* (American Society for Metals, Metals Park, 1967), p. 209.

[3] R. Funk, H. Schachner, C. Triquet, M. Kornmann, and B. Lux, J. Electrochem. Soc. 123, 285 (1976).

[4] S. Ruppi, Int. J. Refract. Met. Hard Mater. 23, 306 (2005).

[5] M. Specht, H. Reisinger, F. Hofman, T. Schulz, E. Landgraf, R.J. Luyken, W. Rösner, M. Grieb, and L. Risch, Solid-State Electron. 49, 716 (2005).

[6] P.D. Ye, B. Yang, K.K. Ng, J. Bude, G.D. Wilk, S. Halder, and J.C.M. Hwang, Appl. Phys. Lett. 86, 063501 (2005).

[7] S. Oh, K. Cicak, R. McDermott, K.B. Cooper, K.D. Osborn, R.W. Simmonds, M. Steffen, J.M. Martinis, and D.P. Pappas, Supercond. Sci. Technol. 18, 1396 (2005).

[8] A.M. Bataille, J.-B. Moussy, F. Paumier, S. Gota, M.-J. Guittet, M. Gautier-Soyer, P. Warin, P. Bayle-Guillemaud, P. Seneor, K. Bouzehouane, and F. Petroff, Appl. Phys. Lett. 86, 012509 (2005).

[9] I. Levin and D. Brandon, J. Am. Ceram. Soc. 81, 1995 (1998).

[10] O. Zywitzki, G. Hoetzsch, F. Fietzke, and K. Goedicke, Surf. Coat. Technol. 82, 169 (1996).

[11] A. Khanna and D.G. Bhat, Surf. Coat. Technol. 201, 168 (2006).

[12] M.A. Lieberman and A.J. Lichtenberg, *Principles of Plasma Discharges and Materials Processing*, 2nd ed. (John Wiley & Sons, Hoboken, 2005), pp. 6-14.

[13] Courtesy of Staffan Swedin.

[14] M.A. Lieberman and A.J. Lichtenberg, *Principles of Plasma Discharges and Materials Processing*, 2nd ed. (John Wiley & Sons, Hoboken, 2005), pp. 308-310.

[15] M. Ohring, *Materials Science of Thin Films*, 2nd ed. (Academic Press, San Diego, 2002), pp. 222-233.

[16] M. Ohring, *Materials Science of Thin Films*, 2nd ed. (Academic Press, San Diego, 2002), pp. 226-227.

[17] U. Helmersson, M. Lattemann, J. Bohlmark, A.P. Ehiasarian, and J.T. Gudmundsson, Thin Solid Films 513, 1 (2006).

[18] W.D. Sproul, D.J. Christie, and D.C. Carter, Thin Solid Films 491, 1 (2005).

[19] S. Berg and T. Nyberg, Thin Solid Films 476, 215 (2005).

[20] T. Nyberg, S. Berg, U. Helmersson, and K. Hartig, Appl. Phys. Lett. 86, 164106 (2005).

[21] M.A. Lieberman and A.J. Lichtenberg, *Principles of Plasma Discharges and Materials Processing*, 2nd ed. (John Wiley & Sons, Hoboken, 2005), pp. 185-203.

[22] M. Birkholz, *Thin Film Analysis by X-Ray Scattering* (Wiley-VCH, Weinheim, 2006), pp. 143-182.

[23] M. Birkholz, *Thin Film Analysis by X-Ray Scattering* (Wiley-VCH, Weinheim, 2006), pp. 37-38.

[24] See, e.g., D.B. Williams and C.B. Carter, *Transmission Electron Microscopy: A Text-book for Materials Science* (Springer, New York, 1996).

[25] J.R. Tesmer and M. Nastasi (Eds.), *Handbook of Modern Ion Beam Materials Analysis* (Materials Research Society (MRS), Pittsburgh, 1995), pp.83-138.

[26] R.M. Martin, *Electronic Structure; Basic Theory and Practical Methods* (Cambridge University Press, Cambridge, 2004).

[27] P. Hohenberg and W. Kohn, Phys. Rev. 136, B864 (1964).

[28] W. Kohn and L.J. Sham, Phys. Rev. 140, A1133 (1965).

[29] http://nobelprize.org/nobel_prizes/chemistry/laureates/1998/

[30] W. Kohn, Rev. Mod. Phys. 71, 1253 (1999).

[31] A.D. Becke, Phys. Rev. A 38, 3098 (1988).

[32] J.P Perdew and Y. Wang, Phys. Rev. B 45, 13244 (1992).

[33] J.P. Perdew, K. Burke, and M. Ernzerhof, Phys. Rev. Lett. 77, 3865 (1996).

[34] D. Vanderbilt, Phys. Rev. B 41, 7892 (1990).

[35] P.E. Blöchl, Phys. Rev. B 50, 17953 (1994).

[36] G. Kresse and D. Joubert, Phys. Rev. B 59, 1758 (1999).

[37] Y. Sato and S. Akimoto, J. Appl. Phys. 50, 5285 (1979).

[38] W.C. Oliver and G.M. Pharr, J. Mater. Res. 7, 1564 (1992).

[39] R.H. French, J. Am. Ceram. Soc. 73, 477 (1990).

[40] W.H. Gitzen, *Alumina as a ceramic material* (The American Ceramic Society, Westerville, 1970), pp. 31, 46, 63-64.

[41] K. Wefers and C. Misra, *Oxides and Hydroxides of Aluminum*, Alcoa Technical Paper No. 19, revised (Alcoa Laboratories, Pittsburgh, 1987).

[42] R.W.G. Wyckoff, *Crystal Structures*, Vol. 2, 2nd ed. (Interscience, New York, 1964), pp. 6-8.

[43] Y.-N. Xu and W.Y. Ching, Phys. Rev. B 43, 4461 (1991).

[44] Y. Yourdshahyan, C. Ruberto, M. Halvarsson, L. Bengtsson, V. Langer, B.I. Lundqvist, S. Ruppi, and U. Rolander, J. Am. Ceram. Soc. 82, 1365 (1999).

[45] G. Gutiérrez, A. Taga, and B. Johansson, Phys. Rev. B 65, 012101 (2001).

[46] M. Sun, A.E. Nelson, and J. Adjaye, J. Phys. Chem. B 110, 2310 (2006).

[47] M. Halvarsson and S. Vuorinen, Surf. Coat. Technol. 76-77, 287 (1995).

[48] Z.-J. Liu, Z.-K. Liu, C. McNerny, P. Mehrotra, and A. Inspektor, Surf. Coat. Technol. 198, 161 (2005).

[49] Z.R. Ismagilov, R.A. Shkrabina, and N.A. Koryabkina, Catal. Today 47, 51 (1999).

[50] D.D. Ragan, T. Mates, and D.R. Clarke, J. Am. Ceram. Soc. 86, 541 (2003).

[51] S. Wang, A.Y. Borisevich, S.N. Rashkeev, M.V. Glazoff, K. Sohlberg, S.J. Pennycook, and S.T. Pantelides, Nature Mater. 3, 143 (2004).

[52] C.S. Bhatia, G. Guthmiller, and A.M. Spool, J. Vac. Sci. Technol. A 7, 1298 (1989).

[53] Y.-S. Min, Y.J. Cho, and C.S. Hwang, Chem. Mater. 17, 626 (2005).

[54] A. Larsson, M. Halvarsson, and S. Ruppi, Surf. Coat. Technol. 111, 191 (1999).

[55] M. Halvarsson and S. Vuorinen, Mater. Sci. Eng. A 209, 337 (1996).

[56] S. Vuorinen and L. Karlsson, Thin Solid Films 214, 132 (1992).

[57] A. Osada, E. Nakamura, H. Homma, T. Hayahi, and T. Oshika, Int. J. Refract. Met. Hard Mater. 24, 387 (2006).

[58] M. Halvarsson and S. Vuorinen, Surf. Coat. Technol. 76-77, 287 (1995).

[59] S. Ruppi and A. Larsson, Thin Solid Films 388, 50 (2001).

[60] A. Larsson and S. Ruppi, Int. J. Refract. Met. Hard Mater. 19, 515 (2001).

[61] J. Müller, M. Schierling, E. Zimmermann, and D. Neuschütz, Surf. Coat. Technol. 120-121, 16 (1999).

[62] J. Skogsmo, M. Halvarsson, and S. Vuorinen, Surf. Coat. Technol. 54-55, 186 (1992).

[63] O. Kyrylov, D. Kurapov, and J.M. Schneider, Appl. Phys. A 80, 1657 (2005).

[64] R. Brill, F. Koch, J. Mazurelle, D. Levchuk, M. Balden, Y. Yamada-Takamura, H. Maier, and H. Bolt, Surf. Coat. Technol. 174-175, 606 (2003).

[65] Y. Yamada-Takamura, F. Koch, H. Maier, and H. Bolt, Surf. Coat. Technol. 142-144, 260 (2001).

[66] J. Rosén, S. Mráz, U. Kreissig, D. Music, and J.M. Schneider, Plasma Chem. Plasma Process. 25, 303 (2005).

[67] R. Cremer, M. Witthaut, D. Neushütz, G. Erkens, T. Leyendecker, and M. Feldhege, Surf. Coat. Technol. 120-121, 213 (1999).

[68] A. Schütze and D.T. Quinto, Surf. Coat. Technol. 162, 174 (2003).

[69] J.M. Schneider, W.D. Sproul, and A. Matthews, Surf. Coat. Technol. 94-95, 179 (1997).

[70] M. Åstrand, T.I. Selinder, F. Fietzke, and H. Klostermann, Surf. Coat. Technol. 188-189, 186 (2004).

[71] J.M. Schneider, W.D. Sproul, A.A. Voevodin, and A. Matthews, J. Vac. Sci. Technol. A 15, 1084 (1997).

[72] J.M. Schneider, W.D. Sproul, and A. Matthews, Surf. Coat. Technol. 98, 1473 (1998).

[73] A. Khanna and D.G. Bhat, Surf. Coat. Technol. 201, 168 (2006).

[74] O. Zywitzki and G. Hoetzsch, Surf. Coat. Technol. 86-87, 640 (1996).

[75] O. Zywitzki and G. Hoetzsch, Surf. Coat. Technol. 94-95, 303 (1997).

[76] Q. Li, Y.-H. Yu, C. Singh Bhatia, L.D. Marks, S.C. Lee, and Y.W. Chung, J. Vac. Sci. Technol. A 18, 2333 (2000).

[77] P. Jin, G. Xu, M. Tazawa, K. Yoshimura, D. Music, J. Alami, and U. Helmersson, J. Vac. Sci. Technol. A 20, 2134 (2002).

[78] J.M. Andersson, Zs. Czigány, P. Jin, and U. Helmersson, J. Vac. Sci. Technol. A 22, 117 (2004).

[79] T. Kohara, H. Tamagaki, Y. Ikari, and H. Fujii, Surf. Coat. Technol. 185, 166 (2004).

[80] J.-H. Choi, D.-Y. Kim, B.J. Hockey, S.M. Wiederhorn, C.A. Handwerker, J.E. Blendell, W.C. Carter, and A.R. Roosen, J. Am. Ceram. Soc. 80, 62 (1997).

[81] A. Marmier and S.C. Parker, Phys. Rev. B 69, 115409 (2004).

[82] J. Ahn and J.W. Rabalais, Surf. Sci. 388, 121 (1997).

[83] J. Toofan and P.R. Watson, Surf. Sci. 401, 162 (1998).

[84] J. Guo, D.E. Ellis, and D.J. Lam, Phys. Rev. B 45, 13647 (1992).

[85] X.-G. Wang, A. Chaka, and M. Scheffler, Phys. Rev. Lett. 84 , 3650 (2000).

[86] Z. Lodziana, J.K. Norskov, and P. Stoltze, J. Chem. Phys. 118, 11179 (2003).

[87] P.J. Eng, T.P. Trainor, G.E. Brown, Jr., G.A. Waychunas, M. Newville, S.R. Sutton, and M.L. Rivers, Science 288, 1029 (2000).

[88] H.P. Pinto, R.M. Nieminen, and S.D. Elliott, Phys. Rev. B 70, 125402 (2004).

[89] M.C. Valero, P. Raybaud, and P. Sautet, J. Phys. Chem. B 110, 1759 (2006).
[90] J.M. McHale, A. Auroux, A.J. Perrotta, and A. Navrotsky, Science 277, 788 (1997).
[91] Z. Lodziana and J.K. Norskov, J. Chem. Phys. 115, 11261 (2001).
[92] I.G. Batyrev and L. Kleinman, Phys. Rev. B 64, 033410 (2001).
[93] Yu.F. Zhukovskii, E.A. Kotomin, N. Herschend, K. Hermansson, and P.W.M. Jacobs, Surf. Sci. 513, 343 (2002).
[94] J. Rosén, J.M. Schneider, and K. Larsson, J. Phys. Chem. B 108, 19320 (2004).
[95] J. Rosén, J.M. Schneider, and K. Larsson, Solid State Commun. 135, 90 (2005).
[96] K. Tominaga, N. Ueshiba, Y. Shintani, and O. Tada, Jpn. J. Appl. Phys. 20, 519 (1981).
[97] K. Tominaga, M. Kume, T. Yuasa, and O. Tada, Jpn. J. Appl. Phys. 24, 35 (1985).
[98] K. Tominaga, S. Iwamura, Y. Shintani, and O. Tada, Jpn. J. Appl. Phys. 21, 688 (1982).
[99] J.M. Andersson, E. Wallin, E.P. Münger, and U. Helmersson, J. Appl. Phys. 100, 033305 (2006).
[100] J.M. Schneider, K. Larsson, J. Lu, E. Olsson, and B. Hjörvarsson, Appl. Phys. Lett. 80, 1144 (2002).
[101] J.M. Schneider, A. Anders, B. Hjörvarsson, I. Petrov, K. Macák, U. Helmersson, and J.-E. Sundgren, Appl. Phys. Lett. 74, 200 (1999).
[102] H. Jonsson, G. Mills, and K.W. Jacobsen in *Classical and Quantum Dynamics in Condensed Phase Simulations*, B.J. Berne, G. Ciccotti, and D.F. Coker (Eds.) (World Scientific, Singapore, 1998).
[103] R.J. Drese and M. Wuttig, J. Appl. Phys. 98, 073514 (2005).